



Nonlinear dislocation motion via nonequilibrium molecular dynamics

William G. Hoover^{a)} and Nathan E. Hoover

Australian National University Computer Centre, Canberra ACT 2600, Australia

William C. Moss

Department of Applied Science, University of California at Davis-Livermore, and Lawrence Livermore Laboratory, Livermore, California 94550

(Received 26 June 1978; accepted for publication 10 August 1978)

Methods are developed to treat the nonlinear propagation of edge dislocations in atomic lattices. Static or low-velocity calculations incorporate Eshelby's analytic solution of the elastic equations. At higher, even transonic velocities, a novel fixed-displacement boundary is used to allow steady-state propagation of edge dislocations. These techniques are applied to crystals with the triangular-lattice structure. The dependence of the Peierls-Nabarro strain and propagation velocity on the range of the forces is studied. Propagation at higher strains and nonlinear effects, transonic dislocation velocities and climb, are also described.

PACS numbers: 62.20.Fe, 61.70.Ga, 62.30.+d

I. INTRODUCTION

The realization that plastic flow occurs through the motion of dislocations has produced a tremendous literature.¹⁻⁵ The cause of dislocation motion is elastic strain. In turn, the motion relieves strain and shear stress. At the time of this conceptual breakthrough in understanding flow, a direct computer simulation of dislocation motion, with realistic forces and crystal structures, lay beyond the capacity of computing machines. The calculations carried out were usually linear and used highly idealized interparticle forces. Conclusions drawn from such calculations cannot be trusted without a painstaking evaluation of their underlying approximations.

At present the problem of propagating dislocations deserves reinvestigation because computers can now treat three-dimensional crystals with thousands of particles and realistic force laws. Progress continues toward finding the force laws between atoms of various kinds,⁶ although much remains to be done.

Because completely realistic problems are so time consuming, it is worthwhile to develop methods for solving them by using the available simpler models. It is in this spirit that we study a model realistic enough to contain the physics of dislocation motion, but still simple enough to permit a thorough exploration of computational techniques. Although our studies involve isolated dislocations, we expect that the single-dislocation results reported here can be incor-

porated in dynamic simulations of many interacting dislocations. These systems can be compared with corresponding continuum models⁷ and used to study high-pressure stress relaxation and work hardening.

The present paper describes work on an atomic scale and is most closely related to that of Sanders, Weiner, and Celli.⁸⁻¹³ The background for the numerical work owes much to Verlet, Alder, and Vineyard¹⁴⁻¹⁶ who developed the numerical methods for calculating macroscopic properties in terms of microscopic Hamiltonians.

Most atomic-scale numerical work on dislocations has followed Weiner's lead in using the Rosenstock-Newell models, in which particles on a square lattice interact through both central and noncentral forces. Our own crystals differ both in structure and in the forces used. We couple the horizontal and vertical directions through central forces and allow motion in both directions. We feel that this complexity is essential for meaningful agreement with experiment.

We discuss here the model, the boundary conditions, and specific techniques useful for determining the propagation characteristics of dislocations. We also point out some independent nonlinear effects observed during the course of this investigation.

II. THE MODEL

The crystals considered here have the triangular lattice structure. The equilibrium vibrational properties for this crystal are known.¹⁷⁻¹⁹ Figure 1 shows the structure. There are three sets of glide planes along which dislocation motion can occur. Each particle has six near neighbors, except in the vicinity of lattice defects. The triangular lattice has the advantage, relative to the square lattice, of mechanical stability when central short-range forces are used. The triangular lat-

^{a)}Fulbright-Hayes Fellow, 1977-1978. This work was partially supported by the Fulbright-Hayes Foundation, by the Lawrence Livermore Laboratory (permanent address), and by the University of California at Davis-Livermore. M.R. Osborne and R.O.W. Watts of the ANU Computer Centre generously provided office space and 50 h of computer time on the Univac 1100/42. Susan G. Murray and Roger W. Brown provided assistance, advice, and 50 h of DEC 10 computer time.

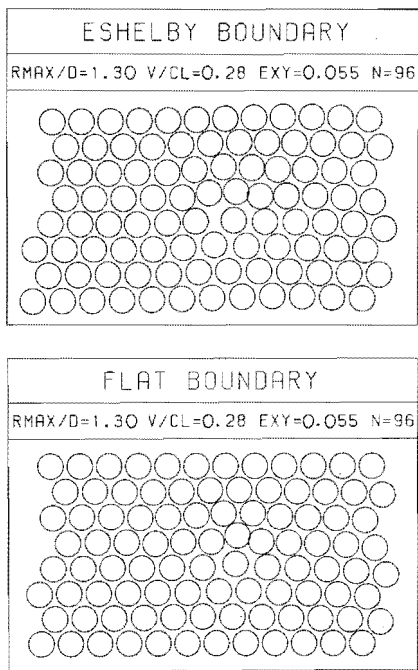


FIG. 1. Two kinds of boundary conditions are illustrated. The boundary particles in the upper crystal strip are displaced according to Eshelby's velocity-dependent solution of the continuum elasticity equations. The upper and lower rows of particles in the lower crystal occupy fixed positions with the crystal boundaries flat. This problem has also been solved in the approximation of continuum elasticity. The flat boundaries are useful in studying dislocation propagation and climb.

tice is also elastically isotropic, facilitating comparisons with continuum elasticity theory. Each particle interacts with its neighbors through a pairwise-additive force law. In most of our work these pairwise forces are piecewise linear.

Because the forces we use are central and allow for motion in both the horizontal and vertical directions, we expect our results to be in reasonable correspondence with those obtained for real crystals. It is of course essential to use not only the correct crystal structure but also realistic repulsive forces in any attempt to correlate model flow calculations with experiments on real materials. We have carried out several dislocation calculations using a representative "realistic" potential in order to indicate the effect of anharmonicity. Linear forces, on the other hand, are unrealistically soft, due to the absence of anharmonic repulsions. One effect of the reduced repulsions is a negative thermal expansion coefficient.²⁰ Nevertheless, linear forces are advantageous in exploratory work, in spite of excessive softness, because the softer linear forces lessen the number dependence of the computed results by reducing the core size.

Both the harmonic and anharmonic interatomic potentials appear in Figure 2. By using the quasiharmonic Einstein approximation to calculate solid-phase properties for the piecewise-linear force law, we can locate the state points reached by shock compression. These equilibrium pressure-volume states are achieved after the original longitudinal stress relaxes through dislocation motion. The details of the relaxation process are crucial to the understanding of high-speed deformation.²¹ So far, computer studies²²⁻²⁴ of solid-

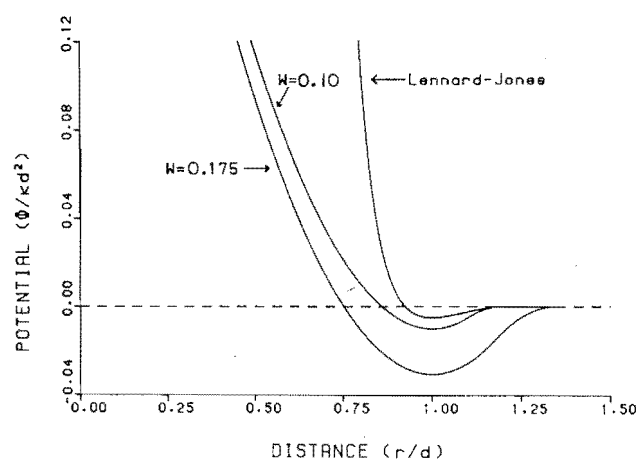


FIG. 2. Interatomic potential functions, $\Phi(r)$, used in dislocation calculations. The two piecewise-linear-force potential functions correspond to attractive-force zeros at d_0 and $d_0 + 2w$. The potentials shown here, for $w/d_0 = 0.10$ and 0.175 , are the extreme members of the set considered. The modified Lennard-Jones potential is also shown. All the potentials we have used have the same force constant κ and the same stress-free density.

phase "shock propagation" have not successfully incorporated dislocation motion and relaxation.

The equation of state for shock compression is found from the equilibrium equation of state. In the piecewise-linear case we have

$$PV/N = \frac{3}{2}\kappa d_0^2(\rho^{-1/2} - \rho^{-1}) + \frac{1}{2}kT(1 - 2\rho^{-1/2})^{-1}; \\ E/N = \frac{3}{2}\kappa d_0^2(\rho^{-1/2} - 1)^2 + 2kT. \quad (1)$$

P , V , T , and E are pressure, volume, temperature, and inter-

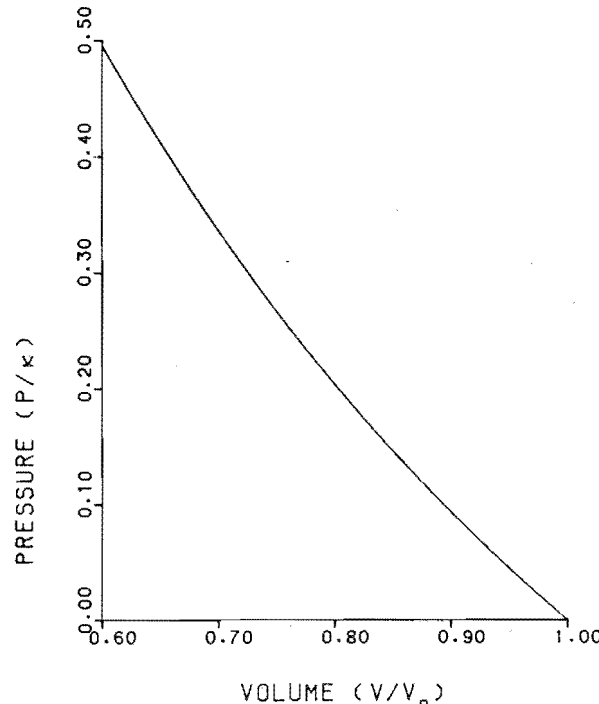


FIG. 3. Hugoniot equation of state for the piecewise-linear-force crystals. The curve represents the pressure-volume states reached by single-shock compression from the static-lattice zero-pressure state. The calculation uses the quasiharmonic approximation to the solid-phase equation of state, and terminates near the melting point.

nal energy. N is the number of particles. The interparticle lattice spacing is d (with d_0 the stress-free zero-temperature value), and $V_0 = \frac{1}{2}\sqrt{3}Nd_0^2$. κ is the Hooke's-law force constant, k is Boltzmann's constant, and ρ is $V_0/V = (d_0/d)^2$. Combining the equation of state (1) with the Hugoniot relation for a material shocked from the stress-free zero-temperature state to a final state with volume V , pressure P , and internal energy E ,

$$E = \frac{1}{2}P(V_0 - V), \quad (2)$$

gives the pressure-volume equation of state shown in Fig. 3. If we use the melting-point estimates discussed below, we find that the melting line crosses the Hugoniot at about 40% compression. In the Lennard-Jones case melting occurs near 25% compression. This means that instantaneous strains of the order of 0.10 can be expected in high-frequency solid-phase deformations.

The piecewise-linear Hugoniot equation of state is qualitatively pathological, in that it lies *below* the zero-temperature isotherm. Fortunately this anomaly, a consequence of negative thermal expansion, is quantitatively unimportant. On the scale of Fig. 3 the Hugoniot and zero-temperature equations of state are nearly indistinguishable from each other. In the Lennard-Jones case about one-third of the melting pressure is thermal.

Our model's soft linear forces extend to a distance ranging arbitrarily from 1.20 to 1.35 times the strain-free interparticle spacing d_0 . The maximum attractive force occurs at half the maximum stretch of $2w$. For real materials, such as the rare gases,⁶ the maximum force occurs at about $1.11d_0$. The Johnson potential for iron²⁵ has a maximum force at $1.17d_0$.

For any w the Lamé constants λ and η are equal. Direct calculation gives the results

$$\lambda = \eta = \frac{1}{4}\sqrt{3}\kappa, \quad (3)$$

where κ is the interparticle potential force constant. The zero-stress transverse and longitudinal sound speeds are $c_t = 0.612$ and $c_l = 1.061$, respectively, in units of $d_0(\kappa/m)^{1/2}$.

An exact correspondence with the Rosenstock-Newell model is impossible because that model sets the elastic constant C_{12} equal to zero.

Microscopic representations of collective macroscopic properties of the crystal model can be used to correlate the atomic and continuum viewpoints. Consider the potential energy, for example. If we write the microscopic potential energy Φ_a of the crystal in terms of the extensions δ of the bonds, we have

$$\Phi_a = \sum_{i < j} \frac{1}{2}\kappa\delta_i^2, \quad (4)$$

valid for extensions less than the maximum-force extension w . If we represent the displacement field $u(r)$ within any (nearly equilateral) triangle of nodal points by the piecewise-linear function

$$u(r) = u_0 + A \cdot r, \quad (5)$$

this microscopic energy [Eq. (4)] is identical to (assuming

the stretches are small with respect to d_0) the "macroscopic" energy calculated from $u(r)$ via continuum elasticity theory,

$$\Phi_c = \frac{1}{2} \int dr \sigma : \epsilon, \quad (6)$$

where σ and ϵ are the stress and strain tensors.²⁶

Another evidence of the close correspondence between the microscopic and macroscopic (atomic and continuum) views of our crystal model can be seen by taking the continuum displacement field to be a piecewise-quadratic function of the locations of the nodal points:

$$u(r) = u_0 + A \cdot r + B : rr. \quad (7)$$

Now consider the equation of motion. The stress divergence gives the nodal accelerations. These follow from the strains, where the coordinates of seven contiguous particles (in the shape of a hexagon) can be used to find u_0 , A , and B in Eq. (7). The set of 14 equations in 12 unknowns has a unique solution if $u_1 + u_3 + u_5 = u_2 + u_4 + u_6$. In this case the resulting *macroscopic* accelerations of the nodal points are *identical* to those calculated as direct vector sums of the *microscopic* interparticle forces.

$$\ddot{u}_c = \rho_m^{-1} \nabla \cdot \sigma = \ddot{u}_a = \sum F/m. \quad (8)$$

In Eq. (8) ρ_m is the mass density and m is the atomic mass.

The similarities in the energy and the accelerations suggest that our microscopic Hamiltonian closely resembles the continuum energy function while still retaining the essential nonlinearities that permit defects to propagate through the atomic lattice.

For real materials the first-neighbor interaction would be fitted to integrated pressure-volume data, and the shear modulus would be most easily described by a noncentral (angle-dependent) force among triples of near neighbors.

The melting transition for our crystal can be estimated by using Ross's analog of Lindemann's (three-dimensional) melting rule²⁷ in two dimensions. Because melting points of two-dimensional crystals have not received much study, we use the rough approximation that the quasiharmonic free-volume integral is equal to the hard-disk free volume²⁸ at the melting point, approximately $0.026d^2$.

III. BOUNDARY CONDITIONS

Eshelby²⁹ calculated the time-dependent displacement field corresponding to the propagation of an edge dislocation in a linear elastic medium. His solution can be used as an external boundary condition and also as an initial guess in atomistic calculations.

For our model, with interparticle force constant κ and mass density $\rho_m = 2\sqrt{3}m/3d^2$, Eshelby's solution takes the form:

$$u_x = (d/\pi)(c_t/v)^2 [\tan^{-1}(\gamma y/x') - \alpha^2 \tan^{-1}(\beta y/x')],$$

$$u_y = (d/\pi)(c_t/v)^2 [\gamma \ln(x'^2 + \gamma^2 y^2)^{1/2}]$$

$$- (\alpha^2/\beta) \ln(x'^2 + \beta^2 y^2)^{1/2}],$$

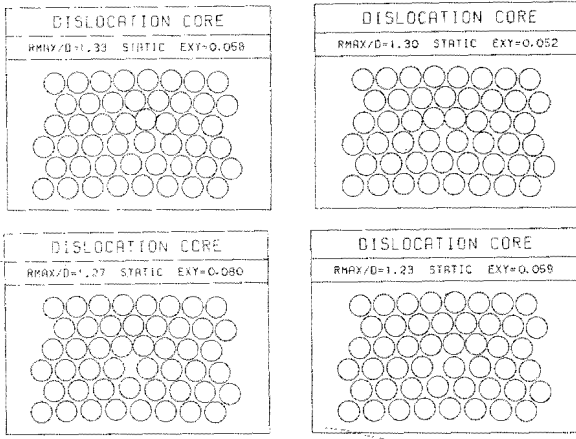


FIG. 4. Dislocation core structures obtained as w/d_0 is reduced from 0.175 to 0.10. The highly strained region in the center contains fewer pairs of interacting particles as the range of the attractive forces is decreased. The structures shown correspond to 0, 1, 2, and 3 "broken" bonds. The Lennard-Jones dislocation core is somewhat wider and corresponds to five or six broken bonds.

$$\begin{aligned}\alpha^2 &= 1 - \frac{1}{2}(v/c_t)^2, \\ \beta^2 &= 1 - (v/c_t)^2, \\ \gamma^2 &= 1 - (v/c_1)^2, \\ c_t^2 &= \frac{3}{8}\kappa d^2/m, \\ c_1^2 &= \frac{9}{8}\kappa d^2/m.\end{aligned}\quad (9)$$

The variable $x' = x - vt$ gives the location of the displacement field (u_x, u_y) relative to an edge dislocation moving at velocity $(v, 0)$.

There are difficulties associated with using Eshelby's solution as a boundary condition. First, it is not known in advance where to place the dislocation in the crystal lattice. Different dislocation cores arise from different choices. Second, it is unknown at what speed the dislocation will travel. If that speed is actually faster than the transverse sound speed, then Eshelby's solution does not exist, while others do. An advantage of the Eshelby solution is that the shear strain vanishes far from the dislocation and the energy of the crystal is only logarithmically divergent with crystal size.

An alternative boundary condition, no more difficult to implement, is the flat boundary used previously to study fracture.³⁰ Here, the strains are nonzero far from the dislocation so that the energy diverges linearly with the system length. It is shown below that for sufficiently large systems the core structure is independent of the chosen boundary conditions. For systems convenient in computer calculations the core-structure number dependence is reduced by using Eshelby's boundary displacements. Flat boundaries are better suited to studying propagation. Boundaries corresponding to fixed stresses are less useful because they lead to nonsteady dislocation propagation.

We have initiated flat-boundary problems in three different ways:

(i) by multiplying Eshelby's solution by $\cos^2(\pi y/2h)$, where $2h$ is the system height;

(ii) by using time-dependent displacements to straighten the crystal boundaries gradually³¹;

(iii) by using the exact solution from elasticity theory³². Method (i) is the simplest.

A relaxation process of some kind must then be used to find the interior initial state consistent with the boundary conditions. A simple way of performing the relaxation is to introduce viscous damping into the equations of motion. Dynamical problems can be similarly started to achieve an approximate steady-state configuration. If the dislocation is assumed to move along the x axis with speed v , then the displacement field depends, in the steady state, on $x' = x - vt$, with x located in the unstrained coordinate system. The acceleration can then be written in terms of the displacement vector u :

$$\ddot{u} \equiv \left(\frac{\partial^2 u}{\partial t^2} \right)_r = \left(\frac{v}{d} \right)^2 (u_{r+d} - 2u_r + u_{r-d}). \quad (10)$$

In order to use Eq. (10) it is convenient to make the further approximation of replacing the second derivative by a centered second difference.

The relaxed configuration actually obtained depends on the way the relaxation is carried out. In practice, even with the simple forces chosen here for systematic study, several initial conditions can be obtained for a given force law, as a result of the relaxation calculation.

Figure 4 shows some of the static core structures found for our piecewise-linear force law. These core structures can conveniently be characterized in terms of the number of pairs of interacting particles. For forces extending to $1.35d_0$ the number of interacting pairs is the same as that in the perfect crystal. For shorter-ranged forces, the number of such interactions can be reduced by 1, 2, 3, ... This increasing reduction corresponds to increasing dislocation core width. To estimate the effect of "realistic" anharmonicity, we have carried out parallel calculations for a modified Lennard-Jones 12-6 potential. Our modification decreases the attractive force to zero linearly between $(13/7)^{1/6}d_0 = d_0 + w$ and $d_0 + 2w$. The Lennard-Jones dislocation core is relatively wide, with five "broken" bonds.

The Rosenstock-Newell model produces a much larger variation of strain with force range and has been applied only to extended dislocation cores. Because the major difference between those calculations⁸⁻¹⁰ and our own is the coupling between the horizontal and vertical displacements, leading to substantial motion (Sec. VI) normal to the glide plane, we believe that the lack of coupling in the oversimplified Rosenstock-Newell calculations is responsible for underestimating the Peierls-Nabarro strains. More definite conclusions will follow from three-dimensional calculations with realistic potentials. The range of dislocation core widths from about d (in the harmonic case) to several times d (in the realistic case) is similar to that found in bubble-raft simulations⁵ by varying the bubble diameter.

IV. PEIERLS-NABARRO STRAINS

The Peierls-Nabarro strain is the minimum shear strain

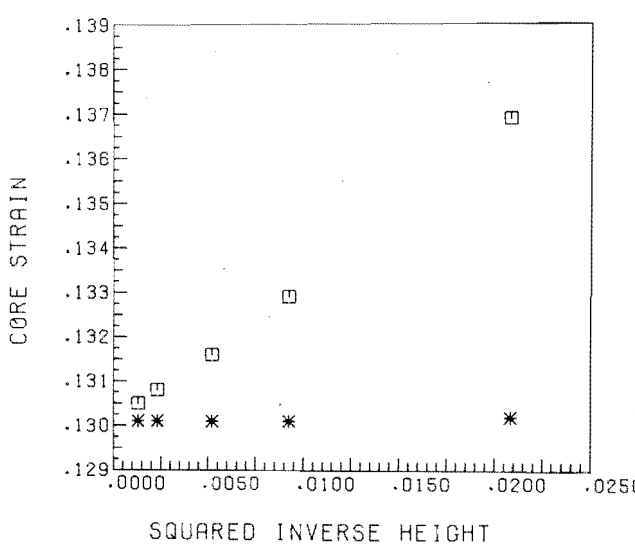


FIG. 5. Variation of strain in the most highly strained bond in a crystal with $w=0.175d_0$. The total height of the system is measured in units of d_0 . All of the points shown correspond to crystals with the same shape ($6n$ columns and $4n$ rows of particles). The data show that core-strain size dependence is greater with flat boundaries (□) than with Eshelby-solution boundaries (*).

required to initiate dislocation motion in a static lattice containing a single dislocation. The strain necessary to propagate a static dislocation depends on the core structure of the dislocation. It is not necessarily the least-energy criterion which determines the core structure. In addition to the viscous damping process, the initial structure of the crystal is required. Dynamical propagation calculations, in which a moving dislocation stops, are reliable guides. We determined core structures by careful study of a series of 24×16 particle crystals with boundaries fixed according to Eshelby's zero-velocity solution of the elastic equations. Figure 5 shows the variation of dislocation core strain with system size. The large-system limiting strain can be obtained within 1% by using a system about 16 atoms wide with flat boundaries and piecewise-linear forces. Using Eshelby's solution a system only half as wide is sufficient. The calculations also show that the core structure reaches the same limit for both types of boundary, even though the displacement field is long range, varying as $\ln r$ far from the dislocation.

The dependence of dislocation core strain on system size, seen in Fig. 5, is less marked than might be expected from the analytic solution for the motion of a screw dislocation through an elastic strip.¹² The analytic solution shows that the strain in a simple cubic crystal bond across the slip plane deviates from the large-system limit by a term of order $1/h$ rather than $1/h^2$, where $2h$ is the height of the crystal.

Strains just below and just above the Peierls-Nabarro strain were imposed on crystals with the dislocation core initially occupying either of two positions separated by half a lattice spacing. We found that for the range of forces considered, $1.20d_0 < d_0 + 2w < 1.35d_0$, only one or two of the possible core structures in Fig. 4 actually occurred as a dislocation came to rest. These structures varied in a systematic way with the range of the forces. See Fig. 4. The determination of core structure is easier with the more realistic wider cores.

To relax the crystal one could use Maxwellian dashpots in parallel with the interatomic forces. This would be equivalent to using a complex force constant in the dynamical calculations. It is much simpler to use Stokes-Einstein damping, as if the particles were immersed in a bath of viscous fluid. Then the equation of motion for each particle has the form

$$m\ddot{u} = \sum F - \zeta \dot{u}, \quad (11)$$

where ζ is a microscopic friction coefficient. The corresponding macroscopic equation of motion is

$$\rho_m \ddot{u} = \nabla \cdot \sigma - \zeta \rho_m \dot{u}/m. \quad (12)$$

It is interesting to see that the damping constant ζ must vary with system size as $1/L$, rather than L , in order to speed convergence for the spectrum of frequencies found in an $L \times L$ system.

Estimates, from 24×16 atom crystals, for the Peierls-Nabarro strain are shown in Fig. 6. Infinite-crystal strains would be slightly lower, particularly for the shorter-range forces. The data points shown would lie on four separate curves. These curves correspond to the four core structures illustrated in Fig. 4. The pentagonal core found with $2w/d_0$ equal to 0.26, 0.27, or 0.28 is particularly stable. Strains higher than one-fourth the theoretical strength of the crystal are required in order to destabilize it. The Peierls-Nabarro strains found are considerably larger than those expected in three-dimensional crystals. As a result considerable energy is stored in the lattice prior to propagation. If we estimate the melting point by setting the two-dimensional hard disk entropy or free volume equal to that calculated (in the harmonic approximation) for our system, we get melting temperatures of 0.016 and 0.012, respectively, in units of $\kappa d_0^2/k$. The stored energy in a crystal at the soft-force Peierls-Nabarro strain corresponds to a few percent of the melting energy, $2NkT_m$. The Lennard-Jones Peierls-Nabarro strain, about 0.006, based on estimates from 96×24 atom crystals, corre-

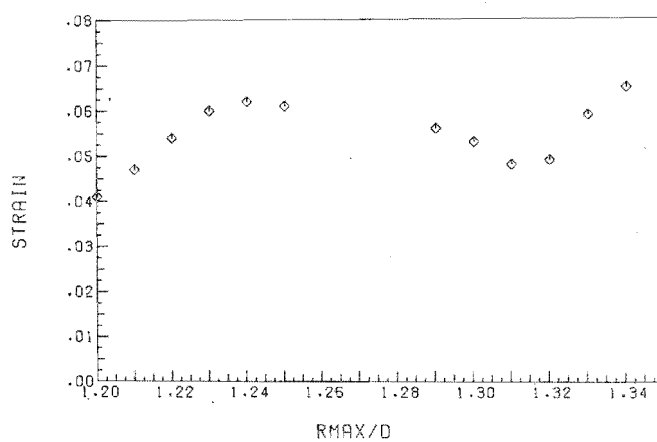


FIG. 6. Variation of Peierls-Nabarro strain with force range. The data shown refer to crystals of $24 \times 16 = 384$ atoms. The boundary particles were fixed at locations given by Eshelby's solution of the elastic equations and the crystals were then allowed to relax for 1500 time steps [$d_0 = 0.1(m/\kappa)^{1/2}$]. Results are not shown for values of $r_{max} = d_0 + 2w$ corresponding to a stable pentagonal dislocation core.

TABLE I. Dislocation propagation results with (i) piecewise-linear forces and (ii) modified 12-6 Lennard-Jones forces. N = columns \times rows is the total number of particles; ϵ is the mean shear strain, du_x/dy ; and v is the steady propagation velocity. The range of the forces r_{\max} is $d_0 + 2w$, with $w/d_0 = (13/7)^{1/6} - 1$ in the modified Lennard-Jones case. In the relaxation phase preceding propagation a friction coefficient of $\zeta = 16(\kappa m)^{1/2}/(\text{number of rows})$ was used. All of these calculations used the flat fixed-displacement boundaries described in the text.

N	r_{\max}/d_0	Piecewise-linear forces			Modified Lennard-Jones		
		ϵ	$v(m/\kappa d^2)^{1/2}$	N	ϵ	$v(m/\kappa d^2)^{1/2}$	
48 \times 8	1.30	0.053	0.32	48 \times 12	0.010	0.61	
		0.060	0.33		0.020	0.96	
48 \times 16		0.053	0.30		0.030	0.97	
		0.060	0.32		0.040	1.10	
		0.070	0.34		0.050	1.11 ^a	
		0.080	0.36		0.050	1.23 ^a	
		0.090	0.38	96 \times 12	0.008	0.41	
		0.100	0.40		0.010	0.45	
64 \times 16		0.060	0.32		0.015	0.71	
					0.020	0.80	
96 \times 16		0.053	0.31		0.030	0.94	
		0.060	0.32		0.040	1.08	
		0.070	0.34		0.050	1.19	
		0.080	0.36				
		0.090	0.39		192 \times 12	0.015	0.75
		0.100	0.40		96 \times 24	0.006	0.34
1.20		0.043	0.35 ^b			0.008	0.36
1.21		0.049	0.35 ^b			0.010	0.37
1.22		0.055	0.36 ^b			0.015	0.41
1.23		0.061	0.32 ^b			0.020	0.47 ^c
1.24		0.064	0.32 ^b			0.020	0.61 ^c
1.25		0.065	0.32			0.030	0.80
1.29		0.062	0.34			0.040	0.94
1.31		0.048	0.29			0.050	1.06
1.32		0.049	0.27	144 \times 36		0.008	0.32
1.33		0.059	0.29				
1.34		0.065	0.30				
1.35		0.074	0.30				

^aVelocity increased after propagating $15d_0$.

^bVelocity prior to structural change.

^cVelocity increased after propagating $20d_0$.

sponds to a stored energy an order of magnitude less relative to the melting transition.

The Peierls-Nabarro strains found limit the dislocation density by excluding dislocations from relatively large areas, particularly in the Lennard-Jones case. Within these areas the shear strains induced are large enough to cause pairs of interacting dislocations either to separate or to annihilate if they occupy the same glide plane. In a clever computer experiment Cotterill studied the saturation of a three-dimensional Lennard-Jones solid with dislocations. By increasing the density of dislocations he was able to model a (possibly metastable) fluid phase.³³

V. PROPAGATION VELOCITY AND CLIMB

A systematic development of macroscopic models for plastic flow involves at least two stages. First, the response of individual dislocations to local stress (stress at the dislocation core) must be determined. At a given stress level, how fast does the dislocation move, and with what effective mass? Second, the collective behavior of many interacting dislocations, treated individually as particles, must be described in an averaged way, in order to simulate work hardening and stress relaxation. Here, we investigate the first of these two

stages, determining the propagation velocity for dislocations at a fixed value of the shear strain.

To study dislocation propagation it is desirable to develop boundary conditions which yield a steady solution. The flat fixed-displacement boundaries will do this and, because these boundaries tend to increase the core strain slightly, are able to propagate dislocations at the Peierls-Nabarro strain found from the Eshelby-solution static calculations.

Our propagation calculations typically make use of a crystal at least four times as long as the crystal height. Exploratory calculations indicate that further lengthening has only a small effect on dislocation velocity when piecewise-linear forces are used. Size effects are much more severe in the anharmonic Lennard-Jones case. See Table I for a compilation of the propagation results.

Each propagation calculation is initiated by allowing a dislocation near one end of the crystal to relax, for a few hundred time steps, using the Stokes-Einstein damping of Eq. (11). Then the friction constant ζ is set to zero and the dislocation is allowed to propagate normally. In a typical case a relatively steady velocity is obtained after a time of five Einstein vibrational periods. The progress of the dislocation down the length of the crystal is most easily followed by

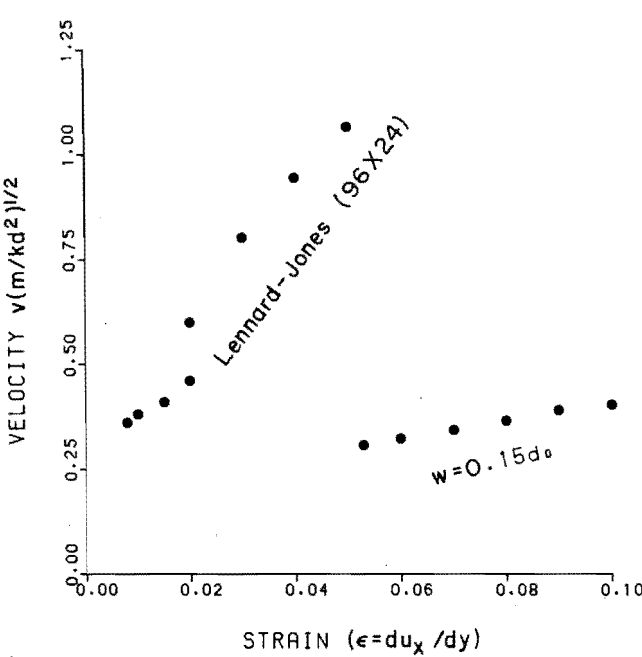


FIG. 7. Variation of velocity with strain for the harmonic potential (with $w=0.15d_0$) and for the modified Lennard-Jones potential (which corresponds to steeper repulsive forces). The size-dependent Lennard-Jones results are shown for a 96×24 particle crystal.

monitoring changes in the relative x separation of two neighboring particles on opposite sides of the glide plane. Fluctuations in propagation velocity are typically small, and an average value can be determined with an uncertainty of $0.01d_0(\kappa/m)^{1/2}$.

The dependence of these average velocities on the range and type of forces can be seen in Table I. For long-range piecewise-linear forces, steady propagation occurs at velocities near one-half the transverse sound speed. For relatively small strains (exceeding the Peierls-Nabarro strain) "normal" propagation occurs and the velocity increases smoothly with strain. Figure 7 illustrates this dependence for both the piecewise-linear and Lennard-Jones forces. Over a sufficiently small range of strain, Gilman's empirical equation,

$$v/c = \exp(\epsilon_0/\epsilon), \quad (13)$$

where c and ϵ_0 are constants, can be used to describe the data. The constants c and ϵ_0 vary from about $\frac{1}{2}c_1$ to more than c_1 , and from 0.01 to 0.03 for the forces we have investigated. (The c appearing in the analogous equation in Ref. 31 refers to the longitudinal rather than transverse sound speed.)

At a given strain the more "realistic" Lennard-Jones forces result in higher velocities. This velocity is also more strain sensitive, presumably because the Lennard-Jones core structure is smoother, as described in Sec. VI. The gross features of the Lennard-Jones data could be described as a power-law dependence, with $v/c \propto \epsilon^{1/3}$. Closer inspection of the data suggests that two different velocity regimes (with a transition, probably depending on system width, linking the two) are involved. Occasionally (two cases are shown in Table I) steady propagation at two different speeds is observed, with a sharp transition between the two, all during a single propagation calculation with $\epsilon = du_x/dy$ fixed.

For any force law the "normal" regime(s) just described must give way to more complex irregularities at sufficiently large strains. Both transonic propagation, at velocities between c_1 and c_1 , and dislocation "climb" can occur. The transonic propagation is not predicted by continuum elasticity (the displacements at the dislocation core diverge at the transverse sound speed in Eshelby's solution). The 96×24 -atom Lennard-Jones results indicate transonic propagation at a strain of 0.02. Distinctly larger strains are required with piecewise-linear forces.

In dislocation climb, another nonlinear phenomenon, the moving "extra" column of particles, which ends at the dislocation, extracts atoms from the lattice, extending the column length and leaving a trail of lattice vacancies behind. Figure 8 illustrates climb for the piecewise-linear forces with $w=0.15d_0$. Normal propagation occurs, in 96×24 -atom strips, for $0.053 < \epsilon < 0.11$. At $\epsilon=0.11$ the vibrational amplitude in the core becomes large enough to form a vacancy in the dilated region below the dislocation (see Fig. 9). In some cases steady climb is observed. The spacing between vacancies in those cases shows that the climb velocity is typically about one-tenth the propagation velocity.

Despite the intrinsic atomic character of climb it is possible to "predict" its occurrence at high speeds from continuum mechanics. A dislocation might be expected to travel in that direction which minimizes the strain energy of the underlying crystal. This direction corresponds to the maximum value of the dislocation's shear stress $\sigma_{r\theta}$. The dependence of $\sigma_{r\theta}$ on velocity and θ , relative to the glide-plane direction, can be obtained directly from Eshelby's solution. One finds that at low velocities, up to about $\frac{1}{2}c_1$, the shear stress is greatest directly ahead of the moving dislocation ($\theta=0$). At higher velocities the maximum shear stress moves to higher angles, reaching the next glide-plane direction ($\theta=\frac{1}{3}\pi$) at about $\frac{1}{2}c_1$. Changes in the direction of maximum tensile stress with velocity have been used to interpret the

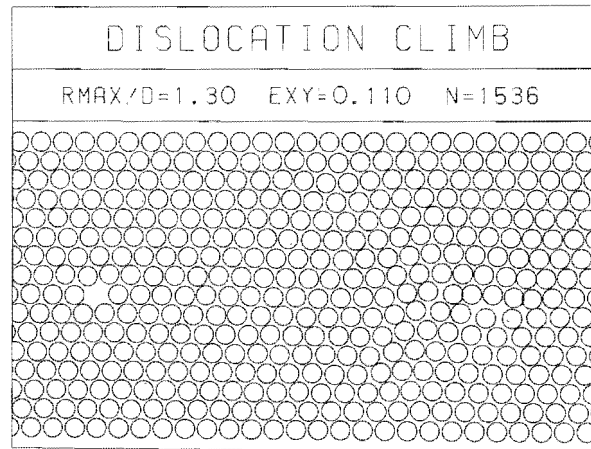


FIG. 8. Snapshot of a crystal illustrating dislocation climb. The dislocation is moving from left to right and was originally gliding along the center line of the crystal. The vacancy near the left-hand side of the figure was created when the moving dislocation extracted the corresponding particle from the crystal and shifted to the next-lower glide plane.

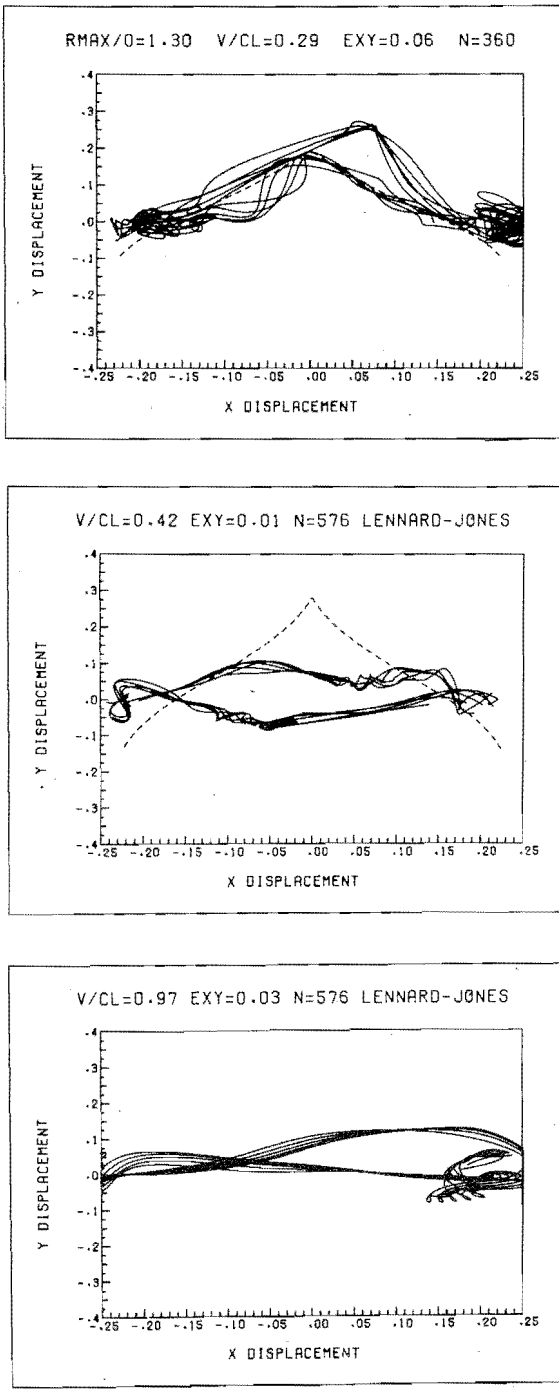


FIG. 9. Particle trajectories near the dislocation core. The dashed lines correspond to Eshelby's analytic solution of the linear-elastic equation of motion. The solid lines are trajectories of 10 particles in a crystalline strip 12 rows high. The upper trajectories are traced out from left to right in the compressed portion of the crystal. The lower trajectories correspond to motion in the dilated region and are traced out from right to left.

irregular movement of cracks in response to tensile stresses.^{34,35}

VI. DYNAMIC CORE STRUCTURE

The approximate dislocation core structure found from continuum mechanics is significantly different in its symmetry from the exact molecular dynamical core structure. Ac-

cording to the continuum point of view, the structure of a moving dislocation is highly symmetric. Individual particle trajectories above and below the glide plane by equal amounts are identical and are also symmetric about the dislocation core. The dashed lines in Fig. 9 show calculated trajectories, from Eshelby's continuum solution, for typical particles lying above (or below) the dislocation glide plane by $(3/16)^{1/2}d_0$. The above-plane trajectories are traced out from left to right with du_x/dt positive. Below-plane displacements are traced out from right to left. The calculated amplitude of the motion normal to the glide plane is relatively large and increases to infinity as v approaches c_r .

In the exact nonlinear computer calculations, actual particle trajectories at low speeds and with soft repulsive forces do resemble the linear-elastic continuum predictions. The piecewise-linear-force trajectories shown in Fig. 9 for $w=0.15d_0$ illustrate this close correspondence. In spite of the close correspondence of the trajectories, three qualitative differences in symmetry can be seen: first, particles in the compressed region above the glide plane are displaced more than are those below; second, there is a marked loss of the time-reversal symmetry of the continuum solution; third, the tangled portions of the trajectories shown in Fig. 9 correspond to thermal vibrations absent from the continuum solution.

In the nearly harmonic case only, the continuum particle trajectories can be used to estimate approximate dislocation propagation velocities. Such estimates are desirable because continuum mechanics by itself cannot select the correct propagation velocity for a particular strain. (All subsonic velocities are possible in the linear continuum theory.) We can estimate propagation velocity by comparing inertial accelerations from continuum trajectories, $\ddot{u}_c \equiv v^2(\partial^2 u / \partial x^2)$, with the accelerations calculated from the interatomic forces, $u_a = F(u)/m$. If we insist that the peak accelerations normal to the glide plane correspond— $\max(\ddot{u}_y)_c = \max(\ddot{u}_y)_a$ —then we obtain a reasonable order-of-magnitude estimate for the velocity v .

With anharmonic interatomic forces, differences between continuum and molecular dynamic trajectories are even greater. As shown in Fig. 9, motion in the vertical (y) direction is reduced, with particles below the glide plane displaced downward as well as upward. In the very-high-velocity regime the trajectories are particularly smooth, and the near symmetry of above-plane and below-plane trajectories is lost.

The flattening of trajectories relative to Eshelby's continuum solution is qualitatively consistent with the high speeds found with steeply anharmonic Lennard-Jones forces. If motion in the perpendicular (y) directions is prevented altogether, by setting u_y equal to zero, then the linear elastic solution

$$u_x = (d/2\pi) \{ \tan^{-1} [\sin y'' / (\exp x'' - \cos y'')] + y'' \},$$

$$x'' = \pi(x - vt) / \sqrt{3\gamma h}; \quad y'' = \pi y/h \quad (14)$$

is essentially (apart from a different scaling of the x axis) that found for a moving screw dislocation.³² The purely longitu-

dinal solution (14) exists for all velocities up to c_1 . As that speed is approached the Lorentz contraction of the x displacement $\gamma = [1 - (v/c_1)^2]^{1/2}$ becomes singular.

VII. CONCLUSIONS

Modern computers can treat the initiation, propagation, and structure of individual edge dislocations in atomistic crystals using realistic interatomic forces. In order to carry out the calculations two different kinds of boundary conditions are useful:

(i) boundaries based on the solution of the linear elastic equation of motion make it possible to use viscous dissipation schemes to determine accurate Peierls-Nabarro strains for the *initiation* of dislocation motion;

(ii) fixed-displacement flat boundaries make it possible to follow steady-state *propagation*, at fixed stress levels, over sufficiently long time intervals for accurate determinations of dislocation velocity and core structure.

The two kinds of boundary conditions predict identical core *structures* for sufficiently large crystallites. At the high strain levels likely to be realized under shock-loading conditions, high propagation velocities are found, particularly with interatomic forces incorporating realistic anharmonicity.

Under thermodynamic conditions that correspond to softer effective interatomic forces the piecewise-linear propagation results lead us to expect slower flow and stress relaxation due to the localized structure of the dislocation core. Extremely stable core structures can result with soft repulsive forces which accentuate the importance of motion perpendicular to the glide plane.

Future studies will focus on the effective mass and drag dissipation in the vicinity of moving dislocations. These studies will enhance our understanding of the materials' deformation by incorporating microscopic calculations into a more nearly macroscopic description of high-frequency plastic flow.

- ¹F.R.N. Nabarro, *Theory of Crystal Dislocations* (McGraw-Hill, New York, 1967).
²J.P. Hirth and J. Lothe, *Theory of Dislocations* (McGraw-Hill, New York, 1969).
³J.J. Gilman, *Micromechanics of Flow in Solids* (McGraw-Hill, New York, 1969).
⁴*Dislocation Dynamics*, edited by A.R. Rosenfield, G.T. Hahn, A.L. Bernstein, and R.I. Jaffee (McGraw-Hill, New York, 1968).
⁵A.H. Cottrell, *Dislocations and Plastic Flow in Crystals* (Oxford U.P., New York, 1953).
⁶I.K. Snook and R.O.W. Watts, *Aust. J. Phys.* **25**, 735 (1972).
⁷R.W. Werne, Ph.D. thesis (Univ. of Calif., Berkeley, 1976) (unpublished).
⁸Y.Y. Earmme and J.H. Weiner, *J. Appl. Phys.* **45**, 603 (1974).
⁹J.H. Weiner and M. Pear, *J. Appl. Phys.* **46**, 2398 (1975).
¹⁰J.H. Weiner and M. Pear, *Philos. Mag.* **31**, 679 (1975).
¹¹W.T. Sanders, *Phys. Rev.* **128**, 1540 (1962).
¹²V. Celli and N. Flytzanis, *J. Appl. Phys.* **41**, 444 (1970).
¹³N. Flytzanis, V. Celli, and A. Nobile, *J. Appl. Phys.* **45**, 5176 (1974).
¹⁴J.P. Hansen and I.R. McDonald, *Theory of Simple Liquids* (Academic, New York, 1976), Chap. 3.
¹⁵J.B. Gibson, A.N. Goland, M. Milgram, and G.H. Vineyard, *Phys. Rev.* **120**, 1229 (1960).
¹⁶B.J. Alder and T.E. Wainwright, *Phys. Rev. Lett.* **18**, 988 (1967).
¹⁷W.G. Hoover, W.T. Ashurst, and R.J. Olness, *J. Chem. Phys.* **60**, 4043 (1974).
¹⁸P. Dean, *Proc. Cambridge Philos. Soc.* **59**, 383 (1963).
¹⁹D.A. Huckaby, *J. Chem. Phys.* **54**, 2910 (1971).
²⁰T.H.K. Barron, *Ann. Phys. (N.Y.)* **1**, 77 (1957).
²¹*Metallurgical Effects at High Strain Rates*, edited by R.W. Rhode, B.M. Butcher, J.R. Holland, and C.H. Karnes (Plenum, New York, 1973).
²²B.L. Holian and G.K. Straub, *Phys. Rev. B* **18**, 1593 (1978).
²³A. Paskin and G.J. Dienes, *J. Appl. Phys.* **43**, 1605 (1972).
²⁴D.H. Tsai and C.W. Beckett, *J. Geophys. Res.* **71**, 2601 (1966).
²⁵R.A. Johnson, *Phys. Rev.* **134A**, 1329 (1964).
²⁶A. Hrennikoff, *J. Appl. Mech.* **8**, A169 (1941).
²⁷W.G. Hoover and M. Ross, *Contemp. Phys.* **12**, 339 (1971).
²⁸W.G. Hoover, N.E. Hoover, and K. Hanson, *J. Chem. Phys.* (to be published).
²⁹J.D. Eshelby, *Proc. Phys. Soc. London* **62A**, 307 (1949).
³⁰W.T. Ashurst and W.G. Hoover, *Phys. Rev. B* **14**, 1465 (1976).
³¹W.G. Hoover, N.E. Hoover, and W.C. Moss, *Phys. Lett. A* **63**, 324 (1977).
³²W.G. Hoover, N.E. Hoover, W.C. Moss, and W.T. Ashurst, *Bull. Am. Phys. Soc.* **22**, 464 (1977); W.C. Moss and W.G. Hoover, *Philos. Mag.* (to be published).
³³R.M.J. Cotterill, W.D. Kristensen, and E.J. Jensen, *Philos. Mag.* **30**, 245 (1974).
³⁴E. Yoffe, *Philos. Mag.* **42**, 739 (1951).
³⁵N.J. Petch, *Fracture*, edited by H. Liebowitz (Academic, New York, 1968), Vol. I, p. 351.